Did the COVID-19 Crisis Reduce Free Tropospheric Ozone across the Northern Hemisphere?

Wolfgang Steinbrecht[1], Dagmar Kubistin[1], Christian Plass-Dulmer[2], David W. Tarasick[3], Jonathan Davies[3], Peter von der Gathen[4], Holger Deckelmann[5], Nis Jepsen[6], Rigel Kivi[7], Norrie Lyall[8], Mathias Palm[9], Justus Notholt[10], Bogumil Kois[11], Peter Oelsner[1], Marc Allaart[12], Ankie Piters[12], Michael Gill[13], Roeland Van Malderen[14], Andy Delcloo[14], Ralf Sussmann[15], Christian Servais[16], Emmanuel Mahieu[16], Gonzague Romanens[17], René Stübi[18], Gerard Ancellet[19], Sophie Godin-Beekmann[19], Shoma Yamanouchi[20], Kimberly Strong[20], Bryan J. J. Johnson[21], Patrick Cullis[22], Irina Petropavlovskikh[23], James W Hannigan[24], Jose-Luis Hernandez[25], Ana Diaz Rodriguez[25], Tatsumi Nakano[26], Thierry Leblanc[27], Fernando Chouza[27], Carlos Torres[28], Omaira García[28], Amelie Röhling[29], Matthias Schneider[29], Thomas Blumenstock[29], Matthew Brian Tully[30], Clare Paton-Walsh[31], Nicholas Brian Jones[31], Richard Querel[32], Susan E Strahan[33], Antje Inness[34], Richard J. Engelen[34], Kai-Lan Chang[35], Owen R. R. Cooper[36], Ryan Michael Stauffer[37], and Anne M. Thompson[38]

[1]Deutscher Wetterdienst
[2]Deutscher Wetterdienst, Meteorologisches Observatorium
[3]Environment and Climate Change Canada
[4]Alfred Wegener Institute, Helmholtz Centre for Polar and Marine Research
[5]Alfred Wegener Institute for Polar and Marine Research
[6]Danish Meteorological Institute
[7]Finnish Meteorological Institute
[8]UK Met Office
[9]University of Bremen
[10]Institute of Environmental Physics, University of Bremen
[11]Institute of Meteorology and Water Management
[12]Royal Netherlands Meteorological Institute
[13]Met Éireann (Irish Met. Service)
[14]Royal Meteorological Institute of Belgium
[15]Karlsruhe Institute of Technology, IMK-IFU
[16]University of Liège
[17]MeteoSwiss
[18]Federal Office of Meteorology and Climatology, MeteoSwiss
[19]LATMOS, CNRS, UVSQ, UPMC
[20]University of Toronto
[21]NOAA ESRL
[22]NOAA ESRL
[23]Cooperative Institute for Research in Environmental Sciences, CU
[24]National Center for Atmospheric Research (UCAR)

[25]Agencia Estatal de Meteorología (AEMET)
[26]Japan Meteorological Agency
[27]Jet Propulsion Laboratory, California Institute of Technology
[28]Agencia Estatal de Meteorología (AEMET), CIAI
[29]Karlsruhe Institute of Technology, IMK-ASF
[30]Bureau of Meteorology
[31]University of Wollongong
[32]National Institute of Water & Atmospheric Research (NIWA)
[33]Universities Space Research Association
[34]ECMWF
[35]Earth System Research Laboratory
[36]Earth System Reserach Laboratory NOAA
[37]NASA Goddard Space Flight Center
[38]NASA-GODDARD

November 26, 2022

Abstract

Throughout spring and summer 2020, ozone stations in the northern extratropics recorded unusually low ozone in the free troposphere. From April to August, and from 1 to 8 kilometers altitude, ozone was on average 7% (˜4 ppbv) below the 2000 to 2020 climatological mean. Such low ozone, over several months, and at so many stations, has not been observed in any previous year since at least 2000. Atmospheric composition re-analyses from the Copernicus Atmosphere Monitoring Service and simulations from the NASA GMI model indicate that the large 2020 springtime ozone depletion in the Arctic stratosphere has contributed less than one quarter to the observed tropospheric anomaly. The observed anomaly is consistent with two recent model simulations, which assume emission reductions similar to those caused by the COVID-19 crisis. COVID-19 related emission reductions appear to be the major cause for the observed low free tropospheric ozone in 2020.

Did the COVID-19 Crisis Reduce Free Tropospheric Ozone across the Northern Hemisphere?

Wolfgang Steinbrecht[1], Dagmar Kubistin[1], Christian Plass-Dülmer[1], Jonathan Davies[2], David W. Tarasick[2], Peter von der Gathen[3], Holger Deckelmann[3], Nis Jepsen[4], Rigel Kivi[5], Norrie Lyall[6], Matthias Palm[7], Justus Notholt[7], Bogumil Kois[8], Peter Oelsner[9], Marc Allaart[10], Ankie Piters[10], Michael Gill[11], Roeland Van Malderen[12], Andy W. Delcloo[12], Ralf Sussmann[13], Emmanuel Mahieu[14], Christian Servais[14], Gonzague Romanens[15], Rene Stübi[15], Gerard Ancellet[16], Sophie Godin-Beekmann[16], Shoma Yamanouchi[17], Kimberly Strong[17], Bryan Johnson[18], Patrick Cullis[18, 19], Irina Petropavlovskikh[18, 19], James Hannigan[20], Jose-Luis Hernandez[21], Ana Diaz Rodriguez[21], Tatsumi Nakano[22], Fernando Chouza[23], Thierry Leblanc[23], Carlos Torres[24], Omaira Garcia[24], Amelie N. Röhling[25], Matthias Schneider[25], Thomas Blumenstock[25], Matt Tully[26], Clare Paton-Walsh[27], Nicholas Jones[27], Richard Querel[28], Susan Strahan[29,30], Ryan M. Stauffer[29,34], Anne M. Thompson[29], Antje Inness[31], Richard Engelen[31], Kai-Lan Chang[32,19], Owen R. Cooper[32,19]

[1]Deutscher Wetterdienst, Hohenpeißenberg, Germany.

[2]Environment and Climate Change Canada, Toronto, Canada.

[3]Alfred Wegener Institut, Potsdam, Germany.

[4]Danish Meteorological Institute, Copenhagen, Denmark.

[5]Finnish Meteorological Institute, Sodankylä, Finland.

[6]British Meteorological Service, Lerwick, United Kingdom.

[7]University of Bremen, Bremen, Germany.

[8]Institute of Meteorology and Water Management, Legionowo, Poland.

[9]Deutscher Wetterdienst, Lindenberg, Germany.

[10]Royal Netherlands Meteorological Institute, DeBilt, The Netherlands.

[11]Met Éireann (Irish Met. Service), Valentia, Ireland.

[12]Royal Meteorological Institute of Belgium, Uccle, Belgium.

[13]Karlsruhe Institute of Technology, IMK-IFU, Garmisch-Partenkirchen, Germany.

[14]University of Liège, Liège, Belgium.

[15]Federal Office of Meteorology and Climatology, MeteoSwiss, Payerne, Switzerland.

[16]LATMOS, Sorbonne Université-UVSQ-CNRS/INSU, Paris, France.

[17]University of Toronto, Toronto, Canada.

[18]NOAA ESRL Global Monitoring Laboratory, Boulder, CO, USA.

[19]Cooperative Institute for Research in Environmental Sciences (CIRES), University of Colorado, Boulder, CO, USA.

[20]National Center for Atmospheric Research, Boulder, CO, USA.

[21]State Meteorological Agency (AEMET), Madrid, Spain.

[22]Meteorological Research Institute, Tsukuba, Japan.

[23]NASA Jet Propulsion Laboratory, California Institute of Technology, Table Mountain Facility, Wrightwood, CA, USA.

[24]Izaña Atmospheric Research Center, AEMET, Tenerife, Spain.

[25]Karlsruhe Institute of Technology, IMK-ASF, Karlsruhe, Germany.

[26]Bureau of Meteorology, Melbourne, Australia.

[27]University of Wollongong, Wollongong, Australia.

[28]National Institute of Water and Atmospheric Research, Lauder, New Zealand.

[29]Earth Sciences Division, NASA Goddard Space Flight Center, Greenbelt, MD, USA.

[30]Universities Space Research Association, Columbia, MD, USA.

[31]European Centre for Medium-Range Weather Forecasts, Reading, United Kingdom.

[32]NOAA Chemical Sciences Laboratory, Boulder, CO, USA.

[33]Earth System Science Interdisciplinary Center, University of Maryland, College Park, MD, USA

Corresponding author: Wolfgang Steinbrecht (wolfgang.steinbrecht@dwd.de)

Key Points:

- From April through August 2020, ozone stations in the northern extratropics report on average 7% (or 4 ppbv) less ozone in the free troposphere than normal.
- Such low tropospheric ozone, over several months, and at so many sites, has not been observed in any previous year since at least the year 2000.
- We suggest that most of the low tropospheric ozone in 2020 is a consequence of the substantial emission reductions caused by decreased worldwide activity due to the COVID-19 pandemic.

Abstract

Throughout spring and summer 2020, ozone stations in the northern extratropics recorded unusually low ozone in the free troposphere. From April to August, and from 1 to 8 kilometers altitude, ozone was on average 7% (≈4 ppbv) below the 2000 to 2020 climatological mean. Such low ozone, over several months, and at so many stations, has not been observed in any previous year since at least 2000. Atmospheric composition re-analyses from the Copernicus Atmosphere Monitoring Service and simulations from the NASA GMI model indicate that the large 2020 springtime ozone depletion in the Arctic stratosphere has contributed less than one quarter to the observed tropospheric anomaly. The observed anomaly is consistent with two recent model simulations, which assume emission reductions similar to those caused by the COVID-19 crisis. COVID-19 related emission reductions appear to be the major cause for the observed low free tropospheric ozone in 2020.

Plain Language Summary

Worldwide actions to curb the spread of the COVID-19 virus have closed factories, grounded airplanes, and have generally reduced travel and transportation. Less fuel was burnt, and less exhaust was emitted into the atmosphere. Due to these measures, the concentration of nitrogen oxides and volatile organic compounds (VOCs) decreased in the atmosphere. These substances are important for photochemical production and destruction of ozone in the atmosphere. In clean or mildly polluted air, reducing nitrogen oxides and/or VOCs will reduce the photochemical production of ozone and result in less ozone. In heavily polluted air, in contrast, reducing nitrogen oxides can increase ozone concentrations, because less nitrogen oxide is available to destroy ozone. In this study, we use data from three types of ozone instruments, but mostly from ozonesondes on weather balloons. The sondes fly from the ground up to 30 kilometers altitude. In the first 10 kilometers we find significantly reduced ozone concentrations in spring and summer of 2020, less than in any other year since at least 2000. We suggest that reduced emissions due to the COVID-19 crisis have lowered photochemical ozone production and have caused the observed ozone reductions in the first 10 kilometers of the atmosphere, the troposphere.

1 Introduction

Widespread slowdowns caused by the COVID-19 pandemic have reduced anthropogenic emissions throughout the year 2020. Guevara et al. (2020) report emission reductions up to 60% for NO_x, and up to 15% for non-Methane Volatile Organic Compounds (NMVOC) over Europe for March and April 2020 (Barré et al., 2020). Based on satellite observations of NO_2 columns (Bouwens et al., 2020), comparable NO_x emission reductions are reported for Chinese cities during February 2020 (Ding et al., 2020; Feng et al., 2020). For the first half of 2020, Liu et al. (2020) report an overall reduction of 8.8% for CO_2 emissions, consistent in magnitude with the mentioned NO_2 emission reductions. The largest relative reductions occurred for airtraffic, where traffic (and emissions) decreased by ≈40% in the first half of 2020 (Liu et al., 2020), and have remained low during the second half of 2020.

COVID 19 emission reductions are large enough to affect ozone levels in the troposphere (Dentener et al., 2011). Tropospheric O_3-NO_x-VOC-HO_x chemistry is, however, complex and non-linear. The net effect of emission changes on ozone depends on NO_x and VOC concentrations, and on their ratios (Kroll et al., 2020; Sillman, 1999; Thornton et al., 2002). In polluted regions, at high NO_x concentrations (>> 1pbb), reducing NO_x concentrations can increase ozone, because ozone titration by NO is reduced (Sicard et al., 2020). At low concentrations (NO_x < 1ppb), however, in the clean or mildly polluted free troposphere, reducing NO_x lowers photochemical ozone production (Bozem et al., 2017) and results in less ozone.

Indeed, for many polluted regions, studies report increased near-surface ozone concentrations after COVID-19 lockdowns (Collivignarelli et al., 2020; Shi & Brasseur, 2020; Siciliano et al., 2020; Venter et al., 2020). Reduced surface ozone is reported for some rural areas after COVID-19 lockdowns, e.g., in the US and Western Europe (Chen et al., 2020; Menut et al., 2020). Meteorological conditions complicate matters, and play an important role as well (Goldberg et al., 2020; Keller et al., 2020; Ordóñez et al., 2020).

In this paper we report significant ozone reductions observed in the free troposphere at many stations in the northern extratropics. These large-scale reductions occurred in late spring and summer 2020, following the widespread COVID-19 slowdowns, and are unique for the last two decades.

2 Instruments and Data

Regular observations of ozone in the free troposphere are sparse: Only around 50 ozone sounding stations worldwide (e.g. Tarasick et al., 2019), a handful of tropospheric lidars (Gaudel et al., 2015; Granados-Muñoz and Leblanc 2016; Leblanc et al., 2018), and about twenty Fourier Transform Infrared Spectrometers (FTIRs, Vigouroux et al., 2015). In-Service Aircraft for a Global Observing System (IAGOS, Nédélec et al., 2015) are another important source of tropospheric ozone data. Due to the COVID-19 slowdowns, however, few IAGOS aircraft were flying in 2020, and IAGOS data became quite sparse. The information content of satellite measurements on ozone in the free troposphere is limited: Typically, only one value (one degree of freedom) for the entire troposphere, with modest accuracy, 10 to 30% (Hurtmans et al., 2012; Liu et al., 2010; Oetjen et al., 2014). The recent Tropospheric Ozone Assessment Report found large differences in tropospheric ozone trends derived from different satellite instruments, and even different signs in some regions (Gaudel et al., 2018).

Ozonesondes measure profiles with high vertical resolution, about 100 m, and good accuracy, about 5 to 15% in the troposphere, 5% in the stratosphere (Smit et al., 2007; Sterling et al., 2018). This is adequate to detect ozone anomalies of several percent. Substantial work has gone into standardizing and improving operating procedures for ozonesondes (WMO, 2014). Homogenization of historical records has started as well (Tarasick et al., 2016; Van Malderen et al., 2016; Witte et al., 2017; Sterling et al., 2018). We use stations with regular soundings, at least once per month since the year 2000, and with data available until at least July 2020. Soundings with obvious deficiencies were rejected (large data gaps, ozone column from the sounding deviating by more than 30% from ground- or satellite-based measurement). Table 1 provides information on stations, and public data archives.

Table 1. Stations in this study, mostly ozonesonde stations. *FTIR and LIDAR stations are italicized*. Data sources: **W**=World Ozone and UV Data Centre (https://woudc.org/archive/Archive-NewFormat/OzoneSonde_1.0_1/), **N**=Network for the Detection of Atmospheric Composition Change (ftp://ftp.cpc.ncep.noaa.gov/ndacc/station/; ftp://ftp.cpc.ncep.noaa.gov/ndacc/RD/), **E**= European Space Agency Validation Data Center (https://evdc.esa.int/ requires registration, or ftp://zardoz.nilu.no/nadir/projects/vintersol/data/o3sondes requires account), **G**=Global Monitoring Laboratory, National Oceanic and Atmospheric Administration (ftp://aftp.cmdl.noaa.gov/data/ozwv/Ozonesonde/)

[1] Currently, Canadian data are available only up to March or April 2020. Newer Canadian data should become available for the final version of this study, and will be included. Newer data from other stations will be included as well for the final version.

[2] Tateno data were corrected for the change from Carbon Iodine to ECC ozonesondes in December 2009.

[3] Stations affected by a drop-off in ECC sonde sensitivity > 3% in the stratosphere, after 2015 (see Stauffer et al., 2020). The drop-off is much smaller (<< 1%) in the troposphere, and should be negligible here. At many of the affected stations, ECC sondes behaved normally again in 2019/2020.

Station	**Latitude (deg N)**	**Longitude (deg E)**	**Data source (see caption)**	**Data until**	**Profiles / spectra per month in 2020**
Alert, Canada [1, 3]	82.50	-62.34	W	4/2020	3.75
Eureka, Canada [1, 3]	80.05	-86.42	W, E	4/2020	5.75
Ny-Ålesund, Norway	78.92	11.92	W, E	8/2020	7.63
Ny-Ålesund FTIR, Norway	*78.92*	*11.92*	*N*	*7/2020*	*12.86*
Thule FTIR, Greenland	*76.53*	*-68.74*	*N*	*9/2020*	*73*
Resolute, Canada [1]	74.72	-94.98	W	4/2020	5.50
Scoresbysund, Greenland	70.48	-21.95	E	9/2020	3.89
Kiruna FTIR, Sweden	*67.41*	*20.41*	*N*	*7/2020*	*46*
Sodankylä, Finland	67.36	26.63	W, E	8/2020	3.00
Lerwick, United Kingdom	60.13	-1.18	W, E	8/2020	4.38
Churchill, Canada [1, 3]	58.74	-93.82	W	3/2020	3.33
Edmonton, Canada [1, 3]	53.55	-114.10	W	3/2020	3.67
Goose Bay, Canada [1]	53.29	-60.39	W	3/2020	2.67
Bremen FTIR, Germany	*53.13*	*8.85*	*N*	*10/2020*	*5.27*
Legionowo, Poland	52.40	20.97	W	10/2020	4.00
Lindenberg, Germany	52.22	14.12	W	10/2020	4.60
DeBilt, Netherlands	52.10	5.18	W, E	8/2020	4.25
Valentia, Ireland	51.94	-10.25	W, E	8/2020	2.75
Uccle, Belgium	50.80	4.36	W, E	8/2020	12.13

Hohenpeissenberg, Germany	47.80	11.01	W	10/2020	10.10
Zugspitze FTIR, Germany	*47.42*	*10.98*	*N*	*9/2020*	*73*
Jungfraujoch FTIR, Switzerland	*46.55*	*7.98*	*N*	*10/2020*	*49*
Payerne, Switzerland	46.81	6.94	W	10/2020	11.10
Haute Provence, France	43.92	5.71	N	8/2020	2.50
Haute Provence LIDAR, France	*43.92*	*5.71*	*N*	*8/2020*	*3.50*
Toronto FTIR, Canada	*43.66*	*-79.40*	*N*	*10/2020*	*59*
Trinidad Head, California, USA	41.05	-124.15	G	8/2020	4.00
Madrid, Spain	40.45	-3.72	W	10/2020	4.10
Boulder, Colorado, USA	39.99	-105.26	G	8/2020	5.13
Boulder FTIR, Colorado, USA	*39.99*	*-105.26*	*N*	*10/2020*	*56*
Tateno (Tsukuba), Japan [2]	36.05	140.13	W	6/2020	3.50
Table Mountain LIDAR, California, USA	*34.40*	*-117.70*	*N*	*8/2020*	*19*
Izana, Tenerife, Spain	28.41	-16.53	W	8/2020	2.00
Izana FTIR, Tenerife, Spain	*28.30*	*-16.48*	*N*	*9/2020*	*28*
Hong Kong, China	22.31	114.17	W	9/2020	4.11
Hilo, Hawaii, USA [3]	19.72	-155.07	G	8/2020	4.00
Mauna Loa FTIR, Hawaii, USA	*19.54*	*-155.58*	*N*	*10/2020*	*36*
Paramaribo, Suriname	5.81	-55.21	N, E	9/2020	3.56
Pago Pago, American Samoa [3]	-14.25	-170.56	G	9/2020	2.67
Suva, Fiji [3]	-18.13	178.32	G	9/2020	1.44
Wollongong FTIR, Australia	*-34.41*	*150.88*	*N*	*10/2020*	*43*
Broadmeadows, Australia	-37.69	144.95	W	7/2020	4.29
Lauder, New Zealand	-45.04	169.68	W	10/2020	4.40
Lauder FTIR, New Zealand	*-45.04*	*169.68*	*N*	*10/2020*	*99*
Macquarie Island, Australia	-54.50	158.94	W	7/2020	4.29

Apart from the sondes, FTIR spectrometers from the Network for the Detection of Atmospheric Composition Change (NDACC, De Mazière et al.,2018) provide independent information, based on a completely different method (ground-based solar-infrared absorption spectrometry). Altitude resolution of FTIR ozone profiles in the troposphere is much coarser (5 to 10 km) compared to the sondes, while accuracy is similar, 5 to 10% (Vigouroux et al.,2015). Finally, we use data from tropospheric lidars (Gaudel et al., 2015, Granados-Muñoz & Leblanc 2016), which provide ozone profiles from ≈3 to 12 km altitude, with accuracy comparable to the sondes (5 to 10%; Leblanc et al., 2018), and slightly coarser altitude resolution (100 m to 2 km).

We also use global atmospheric composition re-analyses from the Copernicus Atmosphere Monitoring Service (CAMS, Inness et al., 2019; see also Park et al., 2020), at the grid-points closest to the stations in Table 1. CAMS re-analyses are based on meteorological fields, and assimilation of satellite observations of ozone and NO_2. They account for the large Arctic stratospheric depletion in spring of 2020 (Manney et al., 2020; Wohltmann et al., 2020), for 2020 meteorological conditions, and for ozone transport, e.g. from the stratosphere to the troposphere (Neu et al., 2014). However, ozone (and NO_2) concentrations in the free troposphere in the CAMS re-analyses are driven primarily by the prescribed emissions. The CAMS re-analyses rely on “business as usual” emissions for 2020, and do not account for COVID 19 emission reductions in 2020. Differences between observations (affected by emission reductions) and CAMS re-analyses (“business as usual” emissions) provide a proxy for the effects of COVID 19 emission reductions.

(Note: at the time of writing, CAMS re-analyses were available until 12/2019. CAMS operational analyses were used to extend the re-analyses from 01/2020 to 10/2020. For the final version of the paper, CAMS re-analyses will be available until at least 06/2020, and will be used).

3 Results

For selected stations, Fig. 1 presents the annual cycles of tropospheric ozone over the last 20 years, at an altitude of 6 km, a representative level for the free troposphere. Monthly means (over 1 km wide layers) reduce synoptic meteorological variability and measurement noise, and focus on longer-term, larger-scale variations.

Payerne and Jungfraujoch measure an annual cycle with low ozone in winter and high ozone in summer. This is the case for most stations in the northern extratropics (Cooper et al., 2014; Gaudel et al., 2018; Parrish et al., 2020). Hilo (Hawaii), and Hongkong (both not shown here), further south and in the Pacific region, have an annual cycle where tropospheric ozone peaks in spring. To a lesser degree this is also seen at Table Mountain (California). At tropical stations and in the Southern Hemisphere (not shown), the annual cycle generally peaks in September or October (=spring in the Southern Hemisphere), and has a smaller amplitude (Cooper et al., 2014; Gaudel et al., 2018; Thompson et al., 2012). Increased photochemical production due to more sunlight and warmer temperatures is the main driver for the summer ozone maximum in the northern extratropics (Wu et al., 2007; Archibald et al., 2020).

Figure 1 shows substantial variations from year to year. Apart from these variations, Fig. 1 shows ozone levels below average in the year 2020 at all four stations (thick red lines in Fig. 1). At Payerne and Jungfraujoch, and a number of other stations, monthly means from February 2020 through August 2020 were actually the lowest, or close to the lowest, since 2000.

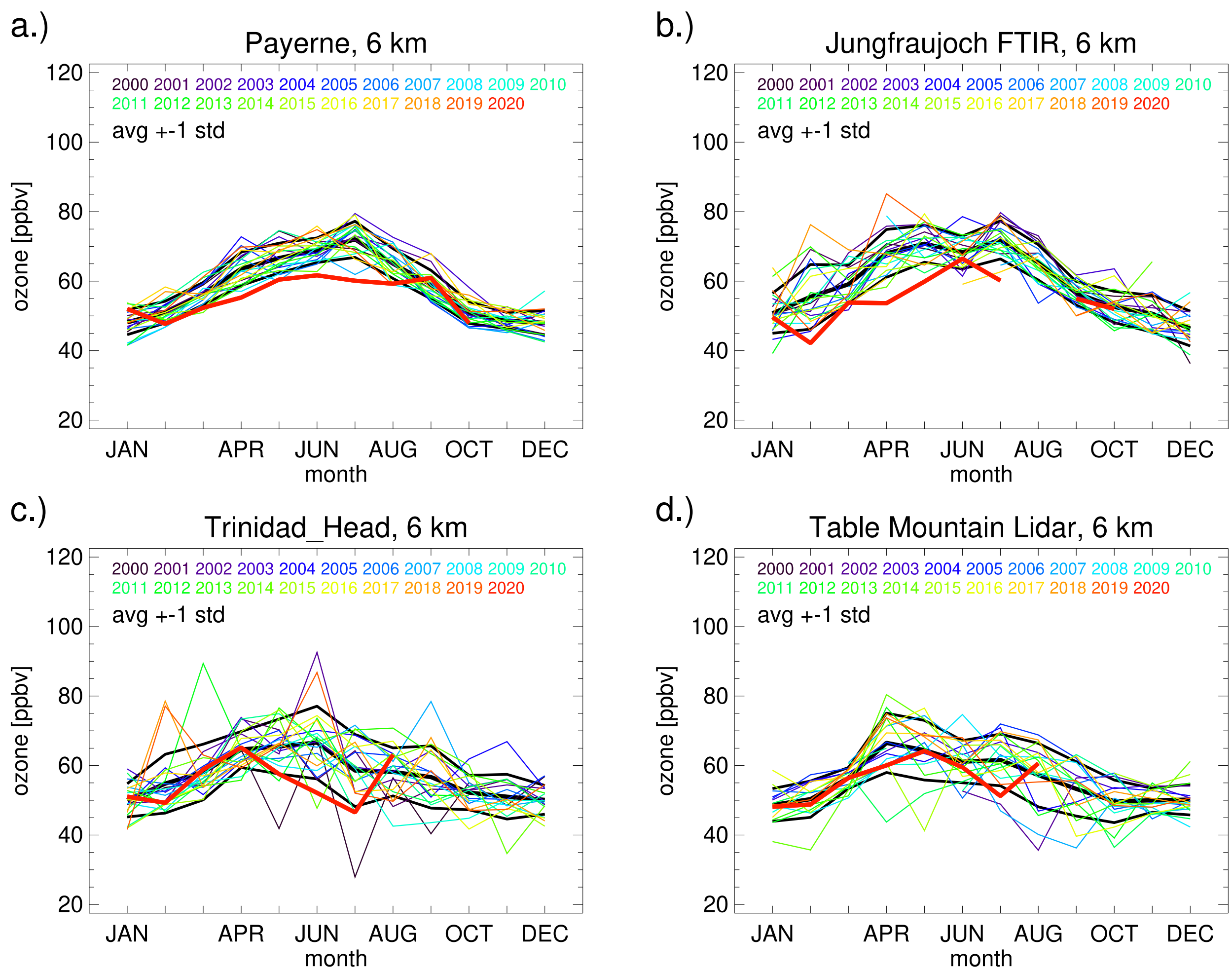

Figure 1. Observed ozone monthly means, from January 2000 to August 2020, and at four typical stations. Results are for 6 km altitude. The thick red line highlights the year 2020. Climatological average, and standard deviation over the years 2000 to 2020 are indicated by the thick black lines. Payerne (**a**) and Trinidad Head (**c**) are sonde stations. Jungfraujoch (**b**) is an FTIR station. Table Mountain (**d**) is a lidar station.

Ozone anomalies as a function of time and altitude are presented in Fig. 2. For clarity, we only show the years 2010 to 2020. Both stations in Fig. 2 show varying positive and negative anomalies at different altitudes. The largest anomalies occur in the 8 to 15 km region, and are caused by meteorological changes, movement of jet streams, changes in tropopause height and location, and large variations of the stratospheric circulation (e.g. Neu et al., 2014). In the troposphere (≈1 to 10 km), the largest and most notable negative anomaly at both stations occurs in 2020 (dark blue region in Fig. 2). This negative anomaly covers several months and most altitudes from 1 to 10 kilometers. Similar significant, extended negative anomalies throughout the troposphere occur at many northern extratropical stations in 2020, but are not seen in previous years, and not across so many locations at the same time.

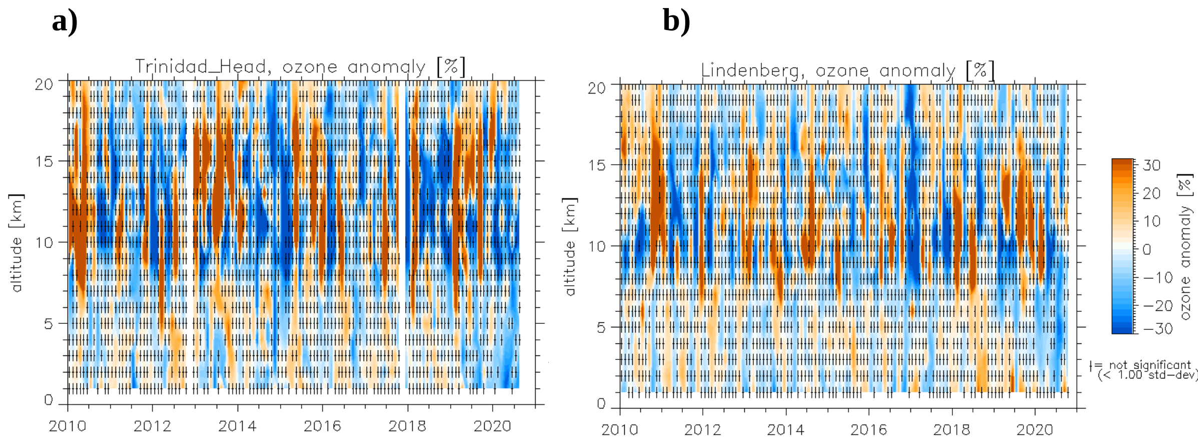

Figure 2. Monthly mean ozone anomalies as a function of altitude and time, for the years 2010 to 2020. Years are labeled with tick marks on January 1st. Panel **a)** is for Trinidad Head. Panel **b)** is for Lindenberg. Anomalies are in percent, relative to the climatological monthly means calculated for the period 2000 to 2020 (all Januaries, all Februaries, …, all Decembers). Anomalies less than 1 standard deviation are crossed out as “insignificant”.

Figs. 1 and 2 show the largest negative anomalies in the troposphere from April to August 2020. Therefore, Fig. 3 compares anomaly profiles averaged over those five calendar months, for the years 2011, and 2020. Both years saw unusually large springtime ozone depletion in the Arctic stratosphere (Manney et al., 2020; Wohltmann et al., 2020). In the stratosphere, above ≈10 km, the Arctic depletion appears as low ozone, both in observations and CAMS results, and particularly for the stations north of 50°N. In both stratosphere and troposphere, the observed profiles are much noisier than the smooth CAMS profiles. In 2020, most observed single station anomaly profiles (Fig. 3b) are negative throughout the troposphere (between 1 and 10 km). This is not the case in 2011 (Fig. 3a, 3c). It is also not reproduced by the CAMS data in 2020 (Fig. 3d).

The difference in 2020 is even clearer for the northern extratropical station average profiles (thick black lines in Fig. 3). The observed 2020 northern extratropical average anomaly is clearly negative, -6% to -9% from 1 to 8 km (Fig. 3b), throughout much of the troposphere, whereas in the CAMS data (Fig. 3d) it is close to zero. Fig. 3 indicates that Arctic stratospheric springtime depletion ozone did not have a large effect on tropospheric ozone in 2011 and 2020, and that the CAMS “business as usual” simulation does not account for the observed large negative tropospheric anomaly in 2020.

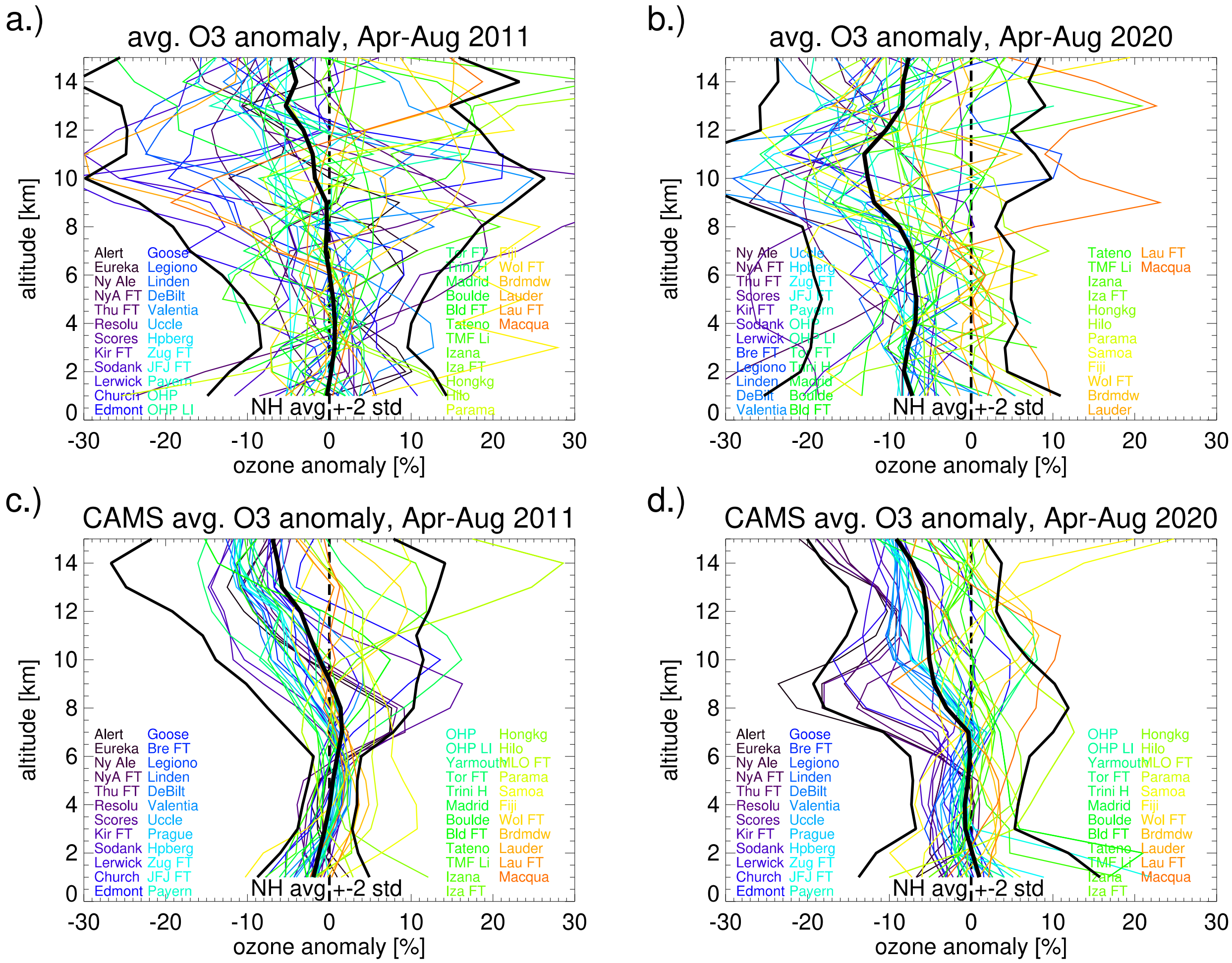

Figure 3. Ozone anomaly profiles (in percent), averaged over the months April to August. Stations are excluded in years where their data cover less than three of these five months. Panel **a)** for the year 2011. Panel **b)** for the year 2020. Colors and stations are sorted by decreasing latitude. Thick black line: average over all stations north of 15°N (=all stations, except Paramaribo, Samoa, Fiji, Wollongong, Broadmeadows, Lauder, Macquarie Island). Thin black lines: ±2 standard deviations around the average. Panels **c), d)**: Same as a), b), but for atmospheric composition re-analyses from CAMS at the grid-points closest to the stations.

Time series of average tropospheric anomalies (averaged from April to August, and now additionally from 1 to 8 km altitude), are shown in Fig. 4. In the observations (left panel) the year 2020 stands out with large negative anomalies. This is not seen in the CAMS data. In almost all twenty previous years, tropospheric ozone anomalies (colored lines) are scattered around zero. The northern extratropical station average (thick black line) is usually smaller than ±3%. The only other exception is the positive anomaly in the (European) heat-wave summer of 2003 (Vautard et al., 2007) in the observations. (The 2003 and 2004 CAMS results might have a low bias). The large negative northern extratropical anomaly in the observations in 2020, ≈-7%, is definitely unique in the 21 year observational record, and is not reproduced by the CAMS "emissions as usual" simulation.

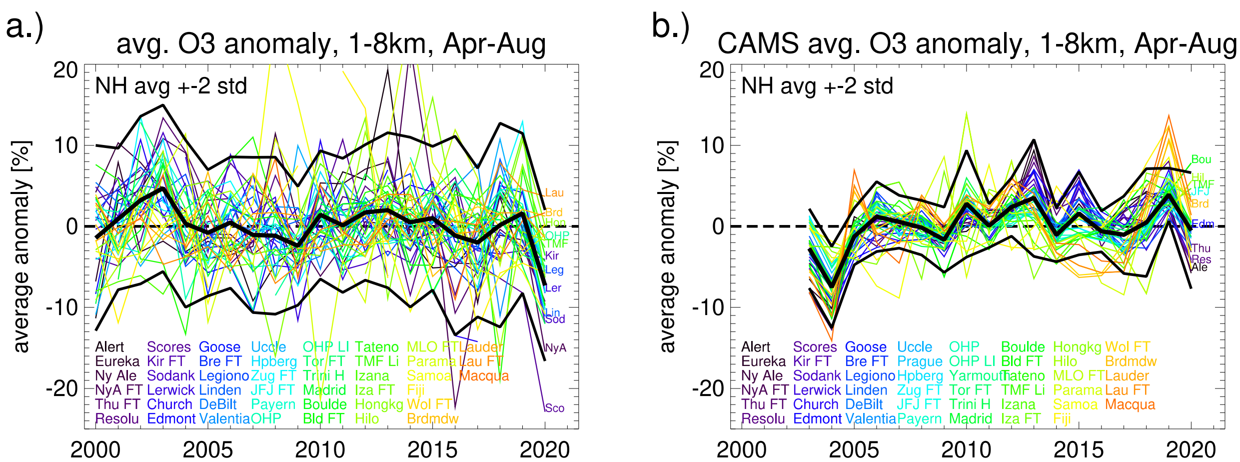

Figure 4. Tropospheric ozone anomaly, averaged over the months April to August and over altitude from 1 to 8 km. Time series for the years 2000 to 2020. Panel **a)** Results from the observations. Panel **b)** same, but for CAMS atmospheric composition re-analyses. Thick black line: Average over all stations north of 15°N. Thin black lines: ±2 standard deviations around the average.

The geographic distribution of the average tropospheric ozone anomalies is shown for 2011 and 2020 in Fig. 5. 2020 stands out in the observations with large negative anomalies at nearly all Northern Hemisphere stations, and a fairly uniform geographical distribution (see Table S1 of the supplement for the numerical values). CAMS does show negative anomalies in 2020, but only north of 50°N, and not as large as the observations. In the Southern Hemisphere in 2020, agreement between observations and CAMS is quite good. In 2011, some stations show positive anomalies. Negative anomalies are not as large as in 2020, and the geographical distribution is less uniform. Agreement between observations and CAMS is reasonable in 2011.

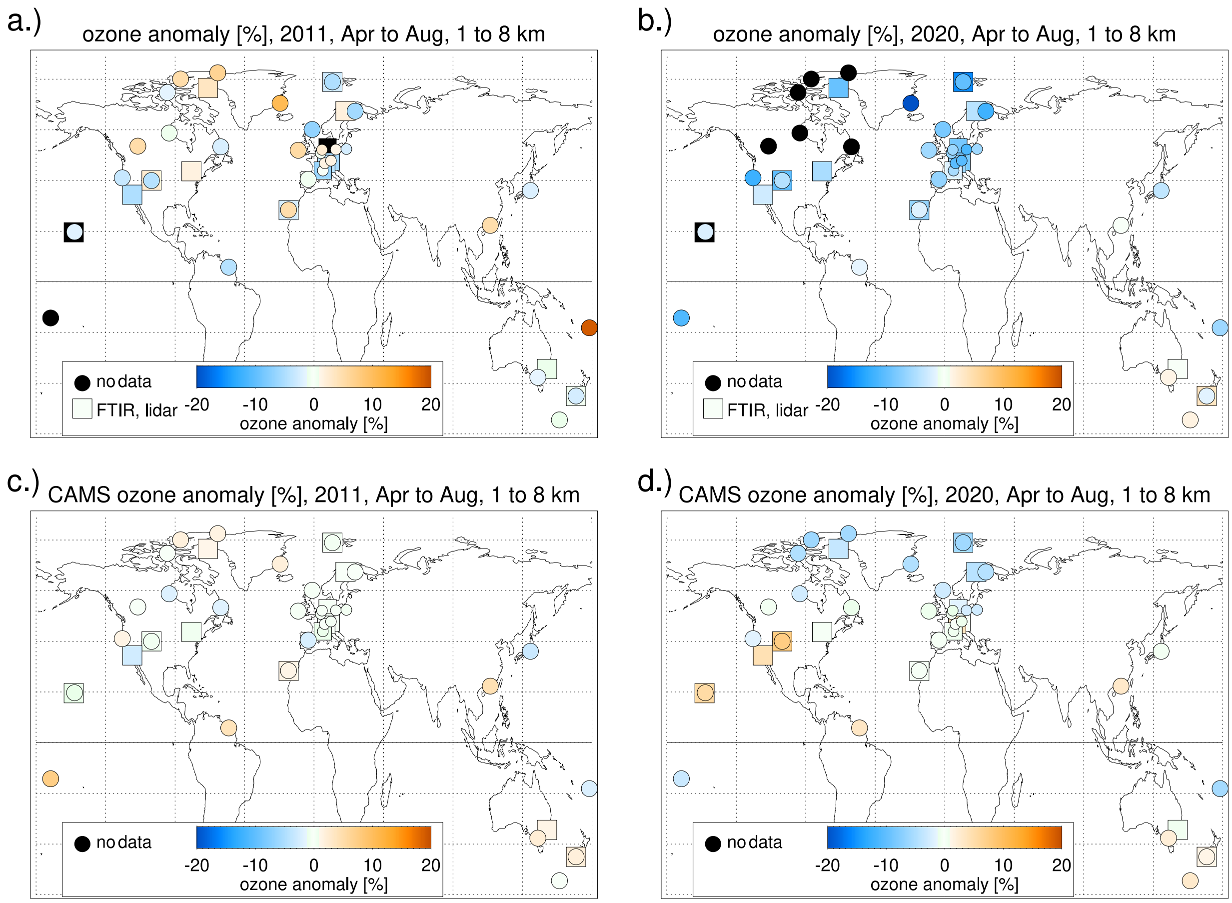

Figure 5. Geographic distribution of observed tropospheric summer ozone anomalies (averaged over the months April to August, and over altitudes from 1 to 8 km) for the years **a)** 2011 and **b)** 2020. Panels **c)** and **d):** same, but for CAMS results at the station locations. Colored circles (or squares) give the anomaly at the ozonesonde stations. Squares are for FTIR and lidar stations. See Table S1 of the supplement for the numerical values. Black filling indicates insufficient data in the given year.

4 Discussion and Conclusions

Ozone stations in the northern extratropics indicate exceptionally low ozone in the free troposphere (1 to 8 km) in spring and summer 2020. Compared to the 2000 to 2020 climatology, ozone was reduced by 7% (≈4 ppbv). Widespread low tropospheric ozone across so many stations and over several months has not been observed in any previous year since 2000. Atmospheric composition re-analyses with “business as usual” emissions from the Copernicus Atmosphere Monitoring Service (CAMS, Inness et al., 2019) do not reproduce the observed low tropospheric ozone in 2020.

The year 2020 stood out in a number of ways: a.) The Arctic stratospheric winter vortex was exceptionally cold and stable. This produced record levels of springtime ozone depletion in the Arctic lower stratosphere (Manney et al., 2020; Wohltmann et al., 2020), which might affect tropospheric ozone (Neu et al., 2014). b.) worldwide measures due to the COVID-19 pandemic caused substantial emission reductions in the Northern Hemisphere, up to 60% for some regions and some sectors (Barré et al., 2020; Bauwens et al., 2020; Ding et al., 2020; Guevara et al., 2020). The largest reductions took place in the first months of the year, but air traffic, for example, remains much reduced throughout 2020 (Liu et al., 2020). c.) large wildfires, in early 2020 in Australia (Kablick et al., 2020), in August and September 2020 in California, with significant pollution. It is unlikely that the Australian fires have affected tropospheric ozone in the northern extratropics, because pollution from these fires did not reach far into the Northern Hemisphere. The California fires were too late to affect April to July ozone values. In any case, emissions from the wildfires should have increased, not reduced, tropospheric ozone (Archibald et al. 2020).

Transport of ozone-depleted air from the Arctic stratospheric vortex appears to be only a minor contributor to the reduced tropospheric ozone: In the observations (Figs. 3 to 5) 2011, and other years with substantial Arctic ozone depletion (2000 and 2016, not shown), do not exhibit large negative anomalies in the troposphere. CAMS atmospheric composition re-analyses also indicate that the 2020 Arctic depletion did not lead to widespread large tropospheric ozone reduction in the northern extratropics (on average less than 1%, see Figs. 3d and 4b). Further evidence for only a small contribution (<1 ppbv, less than one quarter) from the 2020 Arctic depletion to the observed large 7% (or 4 ppbv) reduction comes from the Global Modeling Initiative (GMI) chemistry transport model using MERRA re-analyses (Gelaro et al., 2017; Strahan et al., 2019). See Fig. S2 in the supplement.

Weber et al. (2020) recently simulated global effects of COVID-like emission decreases with the UKCA composition climate model. They find tropospheric ozone reductions very similar to our observational results, both in magnitude and in geographical distribution: Figure 2 of Weber et al. (2020), for example, shows a fairly uniform ozone decrease by 4 to 7% (depending on emission reduction scenario) in the Northern Hemisphere, and no ozone change in the Southern Hemisphere. This is very similar to our results (e.g., Fig. 5b). Analyses based on the NASA GEOS-CF model also project COVID-19 slowdown-related ozone reductions of about 5% for the second half of 2020 (see Fig. 10 of Keller at al., 2020).

We suggest that substantial emission reductions caused by COVID-19 pandemic are the major cause for the observed 7% (or 4 ppbv) reduction of northern extratropical free tropospheric ozone in late spring and summer 2020. The large and continuing reduction in air traffic might be particularly important (Grewe et al., 2017).

Acknowledgments

The authors greatly acknowledge the know-how and the hard work of station personnel launching the ozonesondes and taking the ground-based measurements. Without their dedicated efforts over many years, and especially during the COVID-19 lockdowns in 2020, investigations like this one are not possible!!

Funding acknowledgments

Deutscher Wetterdienst funds the ozone program at Hohenpeißenberg and makes research like this possible.

NOAA GML supported additional launches in Boulder and Trinidad Head in April and May 2020. NOAA and NASA's Upper Atmosphere Composition Observations (UACO) Program support the SHADOZ ozone soundings at Hilo, Pago-Pago (American Samoa) and Suva (Fiji). UACO also provides partial support for the Boulder FTIR and the Table Mountain Lidar.

The NDACC FTIR stations Bremen, Ny-Ålesund, Izaña, Kiruna, and Zugspitze have been supported by the German Bundesministerium für Wirtschaft und Energie (BMWi) via DLR under grants 50EE1711A, 50EE1711B, and 50EE1711D. Zugspitze has also been supported by the Helmholtz Society via the research program ATMO.

The FTIR measurements in Bremen and Ny-Ålesund receive additional support by the Senate of Bremen, the FTIR measurements in Ny-Ålesund also by AWI Bremerhaven. The University of Bremen further acknowledges funding by DFG (German research foundation) TRR 172 – Project Number 268020496 – within the Transregional Collaborative Research Center "ArctiC Amplification: Climate Relevant Atmospheric and SurfaCe Processes, and Feedback Mechanisms (AC)3".

The University of Liège contribution has been supported primarily by the Fonds de la Recherche Scientifique - FNRS under grant J.0147.18, as well as by the CAMS project.

The Toronto FTIR measurements were supported by Environment and Climate Change Canada, the Natural Sciences and Engineering Research Council of Canada (NSERC), and the NSERC CREATE Training Program in Technologies for Exo-Planetary Science.

The University of the Wollongong thanks the Australian Research Council that has provided significant support over the years for the NDACC site at Wollongong, most recently as part of project DP160101598.

Supporting results for this manuscript were generated using Copernicus Atmosphere Monitoring Service Information [2000] from the European Community.

No author reports a financial (or other) conflict of interest.

Data Sources

Most of the ozonesonde data used in this study are freely available from the World Ozone and UV Data Centre (https://woudc.org) at Environment Canada (https://exp-studies.tor.ec.gc.ca/), and are downloadable at https://woudc.org/archive/Archive-NewFormat/OzoneSonde_1.0_1/).

Some ozonesonde data for 2020 were not yet available at the WOUDC. Instead, rapid delivery data were obtained from ftp://zardoz.nilu.no/nadir/projects/vintersol/data/o3sondes (requires registration), at the Nadir database of the Norwegian Institute for Air Quality (NILU, https://projects.nilu.no/nadir/obs.html). Registration information, and the same data in a different format, are available from the European Space Agency Validation Data Center (https://evdc.esa.int/).

For Boulder, Trinidad Head, Hilo, Fiji, and Samoa, stations operated by the US National Oceanic and Atmospheric Administration, Global Monitoring Laboratory (https://www.esrl.noaa.gov/gmd/ozwv/), data can be obtained freely from ftp://aftp.cmdl.noaa.gov/data/ozwv/Ozonesonde/ .

FTIR and lidar data, as well as some ozonesonde data, are from the Network for the Detection of Atmospheric Composition Change (https://ndacc.org), and are freely available at ftp://ftp.cpc.ncep.noaa.gov/ndacc/station/ and ftp://ftp.cpc.ncep.noaa.gov/ndacc/RD/.

Copernicus Atmosphere Monitoring Service (CAMS) global chemical weather re-analyses are available at https://atmosphere.copernicus.eu/data . CAMS operational global analyses and forecasts are available at https://apps.ecmwf.int/datasets/data/cams-nrealtime/ .

References

Archibald, A.T., Neu, J.L., Elshorbany, Y., Cooper, O.R., Young, P.J., Akiyoshi, H., et al. (2020). Tropospheric Ozone Assessment Report: A critical review of changes in the tropospheric ozone burden and budget from 1850-2100. *Elementa Science of the Anthropocene*, in press.

Barré, J., Petetin, H., Colette, A., Guevara, M., Peuch, V.-H., Rouil, L., et al. (in review, 2020). Estimating lockdown induced European NO_2 changes. *Atmospheric Chemistry and Physics Discussions*. https://doi.org/10.5194/acp-2020-995

Bauwens, M., Compernolle, S., Stavrakou, T., Müller, J.-F., van Gent, J., Eskes, H., et al. (2020). Impact of coronavirus outbreak on NO_2 pollution assessed using TROPOMI and OMI observations. *Geophysical Research Letters*, **47**, e2020GL087978. https://doi.org/10.1029/2020GL087978

Bozem, H., Butler, T. M., Lawrence, M. G., Harder, H., Martinez, M., Kubistin, D., et al. (2017). Chemical processes related to net ozone tendencies in the free troposphere. *Atmospheric Chemistry and Physics*, **17**, 10565–10582, https://doi.org/10.5194/acp-17-10565-2017

Chen, L.-W. A., Chien, L.-C., Li, Y., and Lin, G. (2020). Nonuniform impacts of COVID-19 lockdown on air quality over the United States, *Science of The Total Environment*, **745**, 141105. https://doi.org/10.1016/j.scitotenv.2020.141105

Collivignarelli, M.C., Abbà, A., Bertanza, G., Pedrazzani, R., Ricciardi, P., & Carnevale Miino, M. (2020). Lockdown for CoViD-2019 in Milan: What are the effects on air quality? *Science of the Total Environment*, **732**, 139280. https://doi.org/10.1016/j.scitotenv.2020.139280

Cooper, O.R., Parrish, D.D., Ziemke, J., Balashov, N.V., Cupeiro, M., Galbally, I.E., et al. (2014). Global distribution and trends of tropospheric ozone: An observation-based review. *Elementa: Science of the Anthropocene*, **2**, 000029. https://doi.org/10.12952/journal.elementa.000029

De Mazière, M., Thompson, A. M., Kurylo, M. J., Wild, J. D., Bernhard, G., Blumenstock, T., et al. (2018). The Network for the Detection of Atmospheric Composition Change (NDACC): history, status and perspectives. *Atmospheric Chemistry and Physics*, **18**, 4935–4964. https://doi.org/10.5194/acp-18-4935-2018

Dentener F., T. Keating, T., & Akimoto, H. (eds.) (2011). *Hemispheric Transport of Air Pollution 2010, Part A: Ozone and Particulate Matter*. Air Pollution Studies No. 17, United Nations, New York and Geneva, ISSN 1014-4625, ISBN 978-92-1-117043-6. [Available online at http://www.unece.org/index.php?id=25381]

Ding, J., van der A, R. J., Eskes, H. J., Mijling, B., Stavrakou, T., van Geffen, J. H. et al. (2020). NO_x emissions reduction and rebound in China due to the COVID-19 crisis. *Geophysical Research Letters*, **46**, e2020GL089912. https://doi.org/10.1029/2020GL089912

Feng, S., Jiang, F., Wang, H., Wang, H., Ju, W., Shen, Y., et al. (2020). NO_x emission changes over China during the COVID-19 epidemic inferred from surface NO_2 observations. *Geophysical Research Letters*, **47**, e2020GL090080. https://doi.org/10.1029/2020GL090080

Gaudel, A., Ancellet, G., & Godin-Beekmann, S. (2015). Analysis of 20 years of tropospheric ozone vertical profiles by lidar and ECC at Observatoire de Haute Provence (OHP) at 44°N, 6.7°E. *Atmospheric Environment*, **113**, 78-89. https://doi.org/10.1016/j.atmosenv.2015.04.028

Gaudel, A., Cooper, O.R., Ancellet, G., Barret, B., Boynard, A., Burrows, J.P., et al. (2018). Tropospheric Ozone Assessment Report: Present-day distribution and trends of tropospheric ozone relevant to climate and global atmospheric chemistry model evaluation. *Elementa Science of the Anthropocene*, **6**, 39. https://doi.org/10.1525/elementa.291

Gaudel, A., Cooper, O.R., Ziemke, J., Chang, K.-L., Bourgeois, I., Ziemke, J. R., et al. (2020). Aircraft observations since the 1990s reveal increases of tropospheric ozone at multiple locations across the Northern Hemisphere. *Science Advances*, **6**. https://doi.org/10.1126/sciadv.aba8272

Gelaro, R., McCarty, W., Suarez, M. J., Todling, R., Molod, A., Takacs, et al. (2017). The Modern-Era Retrospective Analysis for Research and Applications, version 2 (MERRA-2). *Journal of Climate*, **30**, 5419–5454. https://doi.org/10.1175/JCLI-D-16-0758.1

Goldberg, D. L., Anenberg, S. C., Griffin, D., McLinden, C. A., Lu, Z., & Streets, D. G. (2020). Disentangling the impact of the COVID-19 lockdowns on urban NO_2 from natural variability. *Geophysical Research Letters*, **47**, e2020GL089269. https://doi.org/10.1029/2020GL089269

Granados-Muñoz, M. J., & Leblanc, T. (2016). Tropospheric ozone seasonal and long-term variability as seen by lidar and surface measurements at the JPL-Table Mountain Facility, California. *Atmospheric Chemistry and Physics*, **16**, 9299–9319. https://doi.org/10.5194/acp-16-9299-2016

Grewe, V., Dahlmann, K., Flink, J., Frömming, C., Ghosh, R., Gierens, et al. (2017). Mitigating the Climate Impact from Aviation: Achievements and Results of the DLR WeCare Project. *Aerospace*, **4**, 34, https://doi.org/10.3390/aerospace4030034

Guevara, M., Jorba, O., Soret, A., Petetin, H., Bowdalo, D., Serradell, K., et al. (2020, in review). Time-resolved emission reductions for atmospheric chemistry modelling in Europe during the COVID-19 lockdowns. *Atmospheric Chemistry and Physics Discussions.* https://doi.org/10.5194/acp-2020-686

Hurtmans, D., Coheur, P.-F., Wespes, C., Clarisse, L., Scharf, O., Clerbaux, C., et al. (2012). FORLI radiative transfer and retrieval code for IASI. *Journal of Quantitative Spectroscopy and Radiative Transfer*, **113** (11), 1391-1408. https://doi.org/10.1016/j.jqsrt.2012.02.036.

Inness, A., Ades, M., Agusti-Panareda, A., Barré, J., Benedictow, A., Blechschmidt, A.M., et al. (2019). The CAMS reanalysis of atmospheric composition. *Atmospheric Chemistry and Physics,* **19**, 3515–3556. https://doi.org/10.5194/acp-19-3515-2019

Kablick, G. P., Allen, D. R., Fromm, M. D., & Nedoluha, G. E. (2020). Australian pyroCb smoke generates synoptic-scale stratospheric anticyclones. *Geophysical Research Letters*, **47**, e2020GL088101. https://doi.org/10.1029/2020GL088101

Keller, C. A., Evans, M. J., Knowland, K. E., Hasenkopf, C. A., Modekurty, S., Lucchesi, et al. (in review, 2020). Global Impact of COVID-19 Restrictions on the Surface Concentrations of

Nitrogen Dioxide and Ozone. *Atmospheric Chemistry and Physics Discussions.* https://doi.org/10.5194/acp-2020-685

Kroll, J.H., Heald, C.L., Cappa, C.D., Farmer, D.K., Fry, J.L., Murphy, J.G., & Steiner, A.L. (2020). The complex chemical effects of COVID-19 shutdowns on air quality. *Nature Chemistry*, **12**, 777–779. https://doi.org/10.1038/s41557-020-0535-z

Leblanc, T., Brewer, M. A., Wang, P. S., Granados-Muñoz, M. J., Strawbridge, K. B., Travis, M., et al. (2018). Validation of the TOLNet lidars: the Southern California Ozone Observation Project (SCOOP). *Atmospheric Measurement Techniques*, **11**, 6137–6162. https://doi.org/10.5194/amt-11-6137-2018

Liu, X., Bhartia, P. K., Chance, K., Spurr, R.J.D., & Kurosu, T. P. (2010). Ozone profile retrievals from the Ozone Monitoring Instrument. *Atmospheric Chemistry and Physics*, **10**, 2521–2537. https://doi.org/10.5194/acp-10-2521-2010

Liu, Z., Ciais, P., Deng, Z., Lei, R., Davis, S. J., Feng, S., et al. (2020). Near-real-time monitoring of global CO_2 emissions reveals the effects of the COVID-19 pandemic. *Nature Communications*, **11**, 5172. https://doi.org/10.1038/s41467-020-18922-7

Manney, G. L., Livesey, N. J., Santee, M. L., Froidevaux, L., Lambert, A., Lawrence, Z. D., et al. (2020). Record-low Arctic stratospheric ozone in 2020: MLS observations of chemical processes and comparisons with previous extreme winters. *Geophysical Research Letters*, **47**, e2020GL089063. https://doi.org/10.1029/2020GL089063

Menut, L., Bessagnet, B., Siour, G., Mailler, S., Pennel, R., & Cholakian, A. (2020). Impact of lockdown measures to combat Covid-19 on air quality over western Europe. *Science of The Total Environment*, **741**, 140426. https://doi.org/10.1016/j.scitotenv.2020.140426

Nédélec, P., Blot, R., Boulanger, D., Athier, G., Cousin, J-M., Gautron, B., et al. (2015). Instrumentation on commercial aircraft for monitoring the atmospheric composition on a global scale: the IAGOS system, technical overview of ozone and carbon monoxide measurements. *Tellus B: Chemical and Physical Meteorology*, **67**(1). https://doi.org/10.3402/tellusb.v67.27791

Neu, J., Flury, T., Manney, G., Santee, M.L., Livesey N.J., & Worden, J. (2014). Tropospheric ozone variations governed by changes in stratospheric circulation. *Nature Geosci*ence, **7**, 340–344. https://doi.org/10.1038/ngeo2138

Oetjen, H., Payne, V. H., Kulawik, S. S., Eldering, A., Worden, J., Edwards, D. P., et al. (2014). Extending the satellite data record of tropospheric ozone profiles from Aura-TES to MetOp-IASI: characterisation of optimal estimation retrievals. *Atmospheric Measurement Techniques*, **7**, 4223–4236. https://doi.org/10.5194/amt-7-4223-2014

Ordóñez, C., Garrido-Perez, J.M., & García-Herrera, R. (2020). Early spring near-surface ozone in Europe during the COVID-19 shutdown: Meteorological effects outweigh emission changes. *Science of the Total Environment*, **747**, 141322. https://doi.org/10.1016/j.scitotenv.2020.141322

Park, S., Son, S.-W., Jung, M.-I., Park, J., & Park, S.-S. (2020). Evaluation of tropospheric ozone reanalyses with independent ozonesonde observations in East Asia. *Geoscience Letters.* **7**, 12. https://doi.org/10.1186/s40562-020-00161-9

Parrish, D.D., Derwent, R.G., Steinbrecht, W., Stübi, R., Van Malderen, R., Steinbacher, M., et al. (2020). Zonal similarity of long-term changes and seasonal cycles of baseline ozone at northern midlatitudes. *Journal of Geophysical Research: Atmospheres*, **125**, e2019JD031908. https://doi.org/10.1029/2019JD031908

Sicard, P., De Marco, A., Agathokleous, E., Feng, Z., Xu, X., Paoletti, E., et al. (2020). Amplified ozone pollution in cities during the COVID-19 lockdown, *Science of the Total Environment*, **735**, 139542. https://doi.org/10.1016/j.scitotenv.2020.139542

Siciliano, B., Dantas, G., da Silva, C. M., & Arbilla G. (2020). Increased ozone levels during the COVID-19 lockdown: Analysis for the city of Rio de Janeiro, Brazil, *Science of the Total Environment*, **737**, 139765. https://doi.org/10.1016/j.scitotenv.2020.139765

Sillman, S., (1999). The relation between ozone, NO_x and hydrocarbons in urban and polluted rural environments. *Atmospheric Environment*, **33**(12), 1821-1845. https://doi.org/10.1016/S1352-2310(98)00345-8

Shi, X., & Brasseur, G. P. (2020). The response in air quality to the reduction of Chinese economic activities during the COVID-19 outbreak. *Geophysical Research Letters*, **47**, e2020GL088070. https://doi.org/10.1029/2020GL088070

Smit, H.G.J., Straeter, W., Johnson, B., Oltmans, S., Davies, J., Tarasick, D.W., et al. (2007). Assessment of the performance of ECC-ozonesondes under quasi-flight conditions in the environmental simulation chamber: Insights from the Jülich Ozone Sonde Intercomparison Experiment (JOSIE). *Journal of Geophysical Research*, **112**, D19306. https://doi.org/10.1029/2006JD007308

Stauffer, R.M., Thompson, A.M., Kollonige, D.E., Witte, J.C., Tarasick, D.W., Davies, J., et al. (2020). A post-2013 dropoff in total ozone at a third of global ozonesonde stations: Electrochemical concentration cell instrument artifacts? *Geophysical Research Letters*, **47**, e2019GL086791. https://doi.org/10.1029/2019GL086791

Sterling, C.W., Johnson, D.J., Oltmans, S.J., Smit, H.G.J., Jordan, A.F., Cullis, P.D., et al. (2018). Homogenizing and estimating the uncertainty in NOAA's long-term vertical ozone profile records measured with the electrochemical concentration cell ozonesonde. *Atmospheric Measurement Techniques*, **11**, 3661-3687. https://doi.org/10.5194/amt-11-3661-2018

Strahan, S. E., Douglass, A. R., & Damon, M. R. (2019). Why do Antarctic ozone recovery trends vary? *Journal of Geophysical Research: Atmospheres*, **124**, 8837–8850. https://doi.org/10.1029/2019JD030996

Tarasick, D.W., Davies, J., Smit, H.G.J., & Oltmans, S.J. (2016). A re-evaluated Canadian ozonesonde record: measurements of the vertical distribution of ozone over Canada from 1966 to 2013. *Atmospheric Measurement Techniques*, **9**, 195-214. https://doi.org/10.5194/amt-9-195-2016.

Tarasick, D., Galbally, I.E., Cooper, O.R., Schultz, M.G., Ancellet, G., Leblanc, T., et al. (2019). Tropospheric Ozone Assessment Report: Tropospheric ozone from 1877 to 2016, observed levels, trends and uncertainties. *Elementa Science of the Anthropocene*, **7**(1). https://doi.org/10.1525/elementa.376

Thompson, A. M., Miller, S. K., Tilmes, S., Kollonige, D. W., Witte, J. C., Oltmans, S. J., et al. (2012). Southern Hemisphere Additional Ozonesondes (SHADOZ) ozone climatology (2005-2009): Tropospheric and tropical tropopause layer (TTL) profiles with comparisons to OMI based ozone products. *Journal of Geophysical Research*, **117**, D23301. https://doi.org/10.1029/2010JD016911

Thornton, J.A., Wooldridge, P.J., Cohen, R.C., Martinez, M., Harder, H., Brune, W. H., et al. (2002). Ozone production rates as a function of NO_x abundances and HO_x production rates in Nashville urban plume. *Journal of Geophysical Research*, **107** (D12). https://doi.org/10.1029/2001JD000932

Van Malderen, R., Allaart, M. A. F., De Backer, H., Smit, H. G. J., & De Muer, D. (2016). On instrumental errors and related correction strategies of ozonesondes: possible effect on calculated ozone trends for the nearby sites Uccle and De Bilt. *Atmospheric Measurement Techniques*, **9**, 3793–3816. https://doi.org/10.5194/amt-9-3793-2016

Vautard, R., Beekmann, M., Desplat, J., Hodzic, A., & Morel, S. (2007). Air quality in Europe during the summer of 2003 as a prototype of air quality in a warmer climate. *Comptes Rendus Geoscience*, **339**, 747-763. https://doi.org/10.1016/j.crte.2007.08.003

Venter, Z. S., Aunan, K., Chowdhury, S., & Lelieveld, J. (2020). COVID-19 lockdowns cause global air pollution declines. *Proceedings of the National Academy of Sciences*, **117** (32), 18984-18990. https://doi.org/10.1073/pnas.2006853117

Vigouroux, C, Blumenstock, T, Coffey, M, Errera, Q, García, O, Jones, N.B, et al. (2015). Trends of ozone total columns and vertical distribution from FTIR observations at eight NDACC stations around the globe. *Atmospheric Chemistry and Physics,* **15**, 2915–2933. https://doi.org/10.5194/acp-15-2915-2015

Weber, J., Shin, Y. M., Staunton Sykes, J., Archer-Nicholls, S., Abraham, N. L., & Archibald, A. T. (2020). Minimal climate impacts from short-lived climate forcers following emission reductions related to the COVID-19 pandemic. *Geophysical Research Letters*, **47**, e2020GL090326. https://doi.org/10.1029/2020GL090326

Witte, J. C., Thompson, A.M., Smit, H.G.J., Fujiwara, M., Posny, F., Coetzee G.J.R., et al. (2017). First reprocessing of Southern Hemisphere ADditional OZonesondes (SHADOZ) profile records (1998–2015): 1. Methodology and evaluation. *Journal of Geophysical Research: Atmospheres*, **122**, 6611– 6636. https://doi.org/10.1002/2016JD026403

WMO (2014), *Quality assurance and quality control for ozonesonde measurements in GAW,* World Meteorological Organization (WMO), Global Atmosphere Watch report series, Smit, H.G.J., and ASOPOS panel (eds.), GAW Report No. 201, 100 pp., Geneva. [Available online at https://library.wmo.int/doc_num.php?explnum_id=7167]

Wohltmann, I., von der Gathen, P., Lehmann, R., Maturilli, M., Deckelmann, H., Manney, G. L., et al. (2020). Near-complete local reduction of Arctic stratospheric ozone by severe chemical loss in spring 2020. *Geophysical Research Letters*, **47**, e2020GL089547. https://doi.org/10.1029/2020GL089547

Wu, S., Mickley, L. J., Jacob, D. J., Logan, J. A., Yantosca, R. M., & Rind, D. (2007). Why are there large differences between models in global budgets of tropospheric ozone? *Journal of Geophysical Research*, **112**, D05302. https://doi.org/10.1029/2006JD007801

Young, P. J., Archibald, A. T., Bowman, K. W., Lamarque, J.-F., Naik, V., Stevenson, D. S., et al. (2013). Pre-industrial to end 21st century projections of tropospheric ozone from the

Atmospheric Chemistry and Climate Model Intercomparison Project (ACCMIP). *Atmospheric Chemistry and Physics*, **13**, 2063–2090. https://doi.org/10.5194/acp-13-2063-2013

Geophyscial Research Letters

Supporting Information for

Did the COVID-19 Crisis Reduce Free Tropospheric Ozone across the Northern Hemisphere?

Wolfgang Steinbrecht[1], Dagmar Kubistin[1], Christian Plass-Dülmer[1], Jonathan Davies[2], David W. Tarasick[2], Peter von der Gathen[3], Holger Deckelmann[3], Nis Jepsen[4], Rigel Kivi[5], Norrie Lyall[6], Matthias Palm[7], Justus Notholt[7], Bogumil Kois[8], Peter Oelsner[9], Marc Allaart[10], Ankie Piters[10], Michael Gill[11], Roeland Van Malderen[12], Andy W. Delcloo[12], Ralf Sussmann[13], Emmanuel Mahieu[14], Christian Servais[14], Gonzague Romanens[15], Rene Stübi[15], Gerard Ancellet[16], Sophie Godin-Beekmann[16], Shoma Yamanouchi[17], Kim Strong[17], Bryan Johnson[18], Patrick Cullis[18,19], Irina Petropavlovskikh[18,19], James Hannigan[20], Jose-Luis Hernandez[21], Ana Diaz Rodriguez[21], Tatsumi Nakano[22], Fernando Chouza[23], Thierry Leblanc[23], Carlos Torres[24], Omaira Garcia[24], Amelie N. Röhling[25], Matthias Schneider[25], Thomas Blumenstock[25], Matt Tully[26], Clare Paton-Walsh[27], Nicholas Jones[27], Richard Querel[28], Susan Strahan[29,30], Ryan M. Stauffer[29,34], Anne M. Thompson[29], Antje Inness[31], Richard Engelen[31], Kai-Lan Chang[32,19], Owen R. Cooper[32,19]

[1]Deutscher Wetterdienst, Hohenpeißenberg, Germany.

[2]Environment and Climate Change Canada, Toronto, Canada.

[3]Alfred Wegener Institut, Potsdam, Germany.

[4]Danish Meteorological Institute, Copenhagen, Denmark.

[5]Finnish Meteorological Institute, Sodankylä, Finland.

[6]British Meteorological Service, Lerwick, United Kingdom.

[7]University of Bremen, Bremen, Germany.

[8]Institute of Meteorology and Water Management, Legionowo, Poland.

[9]Deutscher Wetterdienst, Lindenberg, Germany.

[10]Royal Netherlands Meteorological Institute, DeBilt, The Netherlands.

[11]Met Éireann (Irish Met. Service), Valentia, Ireland.

[12]Royal Meteorological Institute of Belgium, Uccle, Belgium.

[13]Karlsruhe Institute of Technology, IMK-IFU, Garmisch-Partenkirchen, Germany.

[14]University of Liège, Liège, Belgium.

[15]Federal Office of Meteorology and Climatology, MeteoSwiss, Payerne, Switzerland.

[16]LATMOS, Sorbonne Université-UVSQ-CNRS/INSU, Paris, France.

[17]University of Toronto, Toronto, Canada.

[18]NOAA ESRL Global Monitoring Laboratory, Boulder, CO, USA.

[19]Cooperative Institute for Research in Environmental Sciences (CIRES), University of Colorado, Boulder, CO, USA.

[20]National Center for Atmospheric Research, Boulder, CO, USA.

[21]State Meteorological Agency (AEMET), Madrid, Spain.

[22]Meteorological Research Institute, Tsukuba, Japan.

[23]NASA Jet Propulsion Laboratory, California Institute of Technology, Table Mountain Facility, Wrightwood, CA, USA.

[24]Izaña Atmospheric Research Center, AEMET, Tenerife, Spain.

[25]Karlsruhe Institute of Technology, IMK-ASF, Karlsruhe, Germany.

[26]Bureau of Meteorology, Melbourne, Australia.

[27]University of Wollongong, Wollongong, Australia.

[28]National Institute of Water and Atmospheric Research, Lauder, New Zealand.

[29]Earth Sciences Division, NASA Goddard Space Flight Center, Greenbelt, MD, USA.

[30]Universities Space Research Association, Columbia, MD, USA.

[31]European Centre for Medium-Range Weather Forecasts, Reading, United Kingdom.

[32]NOAA Chemical Sciences Laboratory, Boulder, CO, USA.

[33]Earth System Science Interdisciplinary Center, University of Maryland, College Park, MD, USA

Corresponding author: Wolfgang Steinbrecht (wolfgang.steinbrecht@dwd.de)

Contents of this file

Text S1 to S2
Figures S1 to S2
Table S1

Introduction

The supplementary material presented here gives additional information on:

- the annual progression of observed and CAMS-simulated ozone anomalies in 2020 and in previous years
- the magnitude of tropospheric ozone reductions that might have been caused by the large springtime ozone depletion of the Arctic stratosphere in 2020.
- the numerical values of the average tropospheric ozone reduction observed in 2020 at the individual stations, and simulated by CAMS at the closest gridpoints.

Text S1.

Figure S1 shows the annual cycle of ozone anomalies observed in the years 2000 to 2020, or simulated by the CAMS re-analyses. The observations show unusual, negative anomalies in 2020, whereas CAMS anomalies in 2020 are within the usual range. The variation over the year 2020 is comparable in observations and CAMS, but the observed monthly anomalies in 2020 are 5 to 10% lower than CAMS. This is attributed to the missing COVID-19 emission reductions in the CAMS simulations, which rely on "business as usual" emissions for 2020. Negative CAMS anomalies from March to May 2020 could indicate tropospheric effects of the large Arctic stratospheric ozone depletion in the spring of 2020.

Text S2.

Figure S2 shows the difference between two simulations by the Global Modeling Initiative (GMI) chemistry transport model (Strahan et al., 2019), based on meteorological fields from MERRA2 re-analysis (Gelaro et al., 2017). One simulation includes the large Arctic ozone depletion caused in spring 2020 by heterogeneous chemistry in the polar vortex; the other simulation does not. The difference between both simulations provides an estimate for the effect of 2020 Arctic stratospheric depletion on ozone in the troposphere. According to the simulations, the tropospheric effect is similar at most latitudes north of 40° to 50°N. It is smaller than 1 ppbv (or ≈2%) on average, and is largest in June 2020.

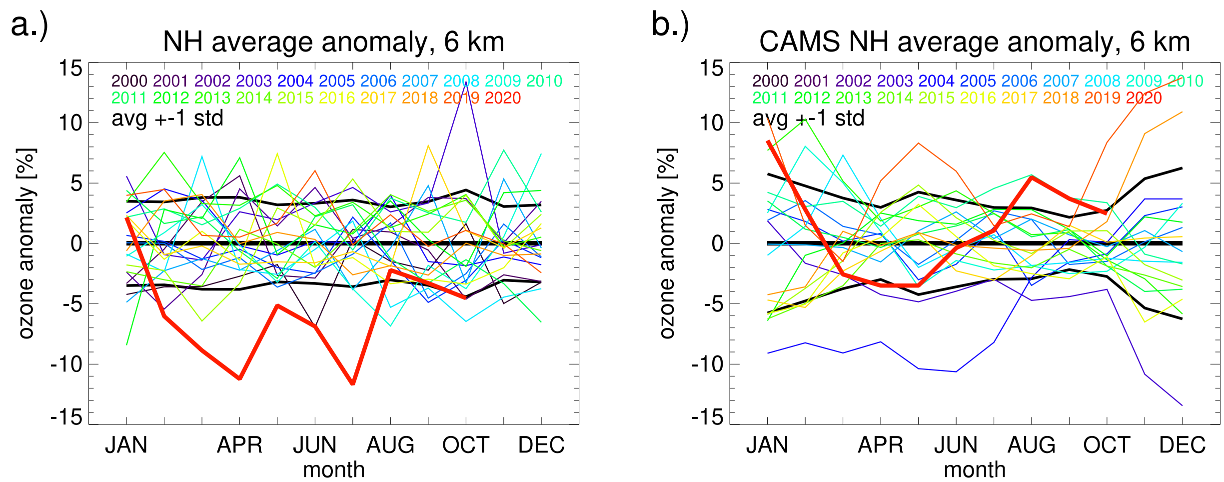

Figure S1. Variation over the year for monthly mean ozone anomalies at 6 km, averaged over all stations north of 15°N (Northern Extra-Tropics). Anomalies are relative to the 2000 to 2020 climatological mean for each calendar month. Colored lines: different years from 2000 to 2020. Thick red line: for the year 2020. Panel a) sonde, FTIR and lidar observations. Panel b) Copernicus Atmosphere Monitoring Service (CAMS) atmospheric composition re-analyses at the grid-points next to the stations. Black lines: average anomaly for each calendar month (zero by definition), and ±1 standard deviations.

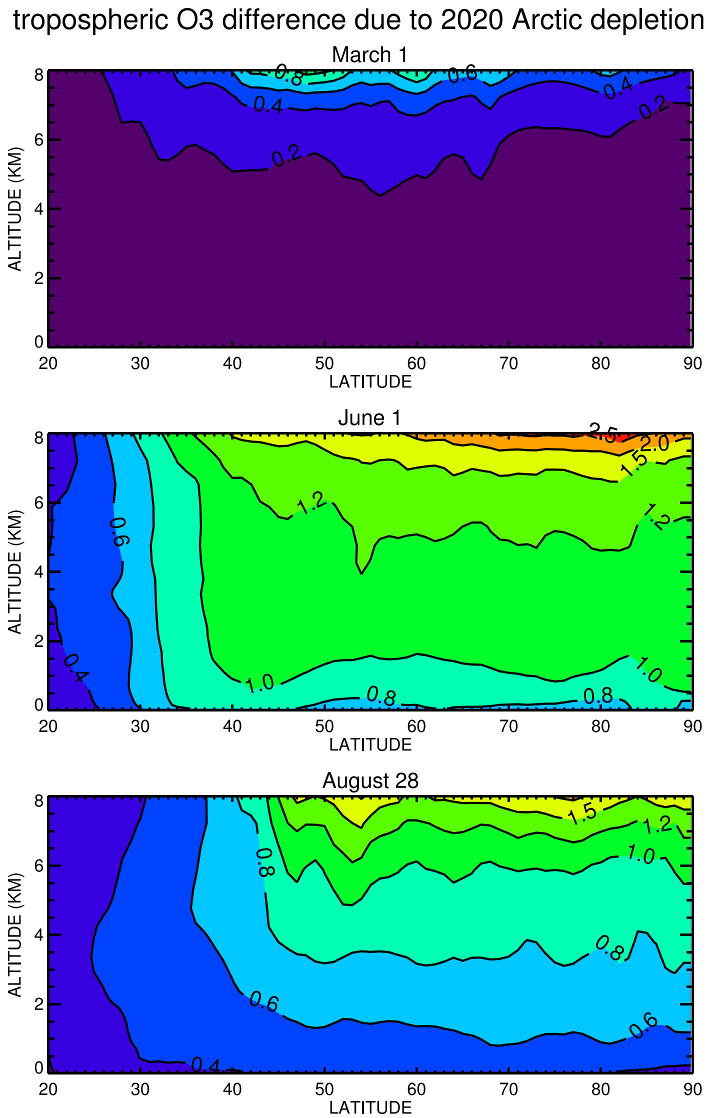

Figure S2. Latitude - altitude cross sections of tropospheric ozone reductions (in ppbv), attributed to the large Arctic springtime stratospheric ozone depletion of 2020. Latitudes go from 20°N to 90°N. Altitudes go from 0 km to 8 km. Top panel is for March 1st, middle panel for June 1st, bottom panel for August 28th. Results are from two simulations by the Global Modeling Initiative (GMI) chemistry transport model (Strahan et al., 2019), based on meteorological fields from the MERRA2 re-analysis (Gelaro et al., 2017). One simulation includes ozone depletion caused by heterogeneous chemistry in the Arctic polar vortex. The other simulation does not. The plotted difference gives an estimate, how much the large Arctic stratospheric ozone depletion in spring 2020 contributed to reduced ozone in the troposphere.

Station	**Latitude (deg N)**	**Longitude (deg E)**	**observed average anomaly 2020 [%]**	**CAMS average anomaly 2020 [%]**
Alert, Canada	82.50	-62.34	N/A	-5.5
Eureka, Canada	80.05	-86.42	N/A	-5.8
Ny-Ålesund, Norway	78.92	11.92	-9.6	-5.5
Ny-Ålesund FTIR, Norway	*78.92*	*11.92*	*-15.5*	*-5.5*
Thule FTIR, Greenland	*76.53*	*-68.74*	*-9.3*	*-3.2*
Resolute, Canada	74.72	-94.98	N/A	-4.5
Scoresbysund, Greenland	70.48	-21.95	-22.9	-4.4
Kiruna FTIR, Sweden	*67.41*	*20.41*	*-4.1*	*-4.1*
Sodankylä, Finland	67.36	26.63	-11.9	-4.2
Lerwick, United Kingdom	60.13	-1.18	-8.0	-2.6
Churchill, Canada	58.74	-93.82	N/A	-2.4
Edmonton, Canada	53.55	-114.10	N/A	-0.2
Goose Bay, Canada	53.29	-60.39	N/A	-0.7
Bremen FTIR, Germany	*53.13*	*8.85*	*-8.2*	*-1.3*
Legionowo, Poland	52.40	20.97	-5.8	-2.6
Lindenberg, Germany	52.22	14.12	-11.1	-2.3
DeBilt, Netherlands	52.10	5.18	-6.0	-0.9
Valentia, Ireland	51.94	-10.25	-5.5	-0.5
Uccle, Belgium	50.80	4.36	-6.6	-0.4
Hohenpeissenberg, Germany	47.80	11.01	-10.3	-0.6
Zugspitze FTIR, Germany	*47.42*	*10.98*	*-8.1*	*0.3*
Jungfraujoch FTIR, Switzerland	*46.55*	*7.98*	*-5.7*	*3.9*
Payerne, Switzerland	46.81	6.94	-10.2	0.2
Haute Provence, France	43.92	5.71	-5.1	-0.5
Haute Provence LIDAR, France	*43.92*	*5.71*	*-1.6*	*-0.5*
Toronto FTIR, Canada	*43.66*	*-79.40*	*-4.9*	*-0.1*
Trinidad Head, California, USA	41.05	-124.15	-12.0	-1.3
Madrid, Spain	40.45	-3.72	-6.3	0.4
Boulder, Colorado, USA	39.99	-105.26	-4.3	7.8
Boulder FTIR, Colorado, USA	*39.99*	*-105.26*	*-9.8*	*7.8*
Tateno (Tsukuba), Japan	36.05	140.13	-3.6	0.5
Table Mountain LIDAR, California, USA	*34.40*	*-117.70*	*-2.6*	*4.7*
Izana, Tenerife, Spain	28.41	-16.53	-1.6	0.0

Izana FTIR, Tenerife, Spain	*28.30*	*-16.48*	*-6.3*	*0.0*
Hong Kong, China	22.31	114.17	0.0	3.2
Hilo, Hawaii, USA	19.72	-155.07	-1.7	5.6
Mauna Loa FTIR, Hawaii, USA	*19.54*	*-155.58*	*N/A*	*5.6*
Northern extratropical station average ±standard deviation	50.94 ±16.98	-29.57 ±66.63	**-7.5 ±4.6**	**-0.5 ±3.6**
Paramaribo, Suriname	5.81	-55.21	-1.0	3.6
Pago Pago, American Samoa	-14.25	-170.56	-10.8	-3.0
Suva, Fiji	-18.13	178.32	-5.8	-5.2
Wollongong FTIR, Australia	*-34.41*	*150.88*	*0.3*	*0.8*
Broadmeadows, Australia	-37.69	144.95	1.3	2.3
Lauder, New Zealand	-45.04	169.68	-1.4	1.4
Lauder FTIR, New Zealand	*-45.04*	*169.68*	*3.7*	*1.4*
Macquarie Island, Australia	-54.50	158.94	1.7	3.0
Tropical and Southern Hemisphere station average ±standard deviation	-30.41 ±20.00	93.33 ±131.40	**-1.5 ±4.7**	**0.5 ±3.1**

Table S1. Similar to Table 1, but showing the average April to August, 1 to 8 km, tropospheric ozone anomaly observed in 2020 at each station, and simulated at the CAMS grid-point next to the station. Two additional rows (**bold-face**) show the 2020 tropospheric anomaly averaged over all northern extratropical stations, and averaged over Tropical and Southern Hemisphere stations.